European Journal of Radiology 83 (2014) 1250–1256

Contents lists available at ScienceDirect

European Journal of Radiology

journal homepage: www.elsevier.com/locate/ejrad

Differentiation between *vasogenic-edema* versus *tumor-infiltrative* area in patients with glioblastoma during bevacizumab therapy: A longitudinal MRI study

Moran Artzi[a,b,1], Felix Bokstein[c,2], Deborah T. Blumenthal[c,3], Orna Aizenstein[a,4], Gilad Liberman[a,d,5], Benjamin W. Corn[a,e,6], Dafna Ben Bashat[a,b,f,*]

[a] *Functional Brain Center, Tel Aviv Sourasky Medical Center, Tel Aviv, Israel*
[b] *Sackler Faculty of Medicine, Tel Aviv University, Tel Aviv, Israel*
[c] *Neuro-Oncology Service, Tel Aviv Sourasky Medical Center, Tel Aviv, Israel*
[d] *Gonda Multidisciplinary Brain Research Center, Bar Ilan University, Ramat Gan, Israel*
[e] *Institute of Radiotherapy, Tel Aviv Sourasky Medical Center, Tel Aviv, Israel*
[f] *Sagol School of Neuroscience, Tel Aviv University, Tel Aviv, Israel*

ARTICLE INFO

Article history:
Received 23 October 2013
Received in revised form 20 March 2014
Accepted 22 March 2014

Keywords:
Glioblastoma
Bevacizumab
Vasogenic-edema
Tumor-infiltrative areas
RANO criteria

ABSTRACT

Background: Treatment with bevacizumab is associated with substantial radiologic response in patients with glioblastoma (GB). However, following this initial response, changes in T_2-weighted MRI signal may develop, suggesting an infiltrative pattern of tumor progression. The aim of this study was to differentiate between *vasogenic-edema* versus *tumor-infiltrative* area in GB patients.
Methods and materials: Fourteen patients with GB were longitudinally scanned, before and during intravenous bevacizumab therapy (5/10 mg/kg every 2-weeks). A total of 40 MR scans including conventional, diffusion, dynamic susceptibility contrast, dynamic contrast enhancement imaging, and MR-spectroscopy (MRS) were analyzed. Classification of non-enhancing fluid-attenuation-inversion-recovery (FLAIR) area was performed based on mean diffusivity, cerebral blood volume and flow maps, and further characterized using multiple MRI parameters.
Results: The non-enhancing FLAIR lesion area was classified into: *vasogenic-edema*, characterized by reduced perfusion and increased FLAIR values; or *tumor-infiltrative* area, characterized by increased perfusion. *Tumor-infiltrative* area demonstrated a higher malignant pattern on MRS compared to areas of *vasogenic-edema*. Substantial reductions of the enhanced T_1-weighted ($58 \pm 10\%$) and hyperintense FLAIR ($53 \pm 9\%$) lesion volumes were detected mainly during the first weeks of therapy, with a shift to an infiltrative pattern of tumor progression thereafter, as detected by an increase in *tumor-infiltrative* area in the majority of patients, which correlated with progression-free survival (week 8: $r = -0.86$, $p = 0.003$, week 16: $r = -0.99$, $p = 0.001$).
Conclusion: Characterization of non-enhancing hyperintense FLAIR lesion area in GB patients can provide an MR-based biomarker, indicating a shift to an infiltrative progression pattern, and may improve therapy response assessment in patients following bevacizumab therapy.

* Corresponding author at: Functional Brain Center, Tel Aviv Sourasky Medical Center, Tel Aviv, Israel. Tel.: +972 3 6973056/+972 52 4262515; fax: +972 3 6973080.
E-mail addresses: artzimy@gmail.com (M. Artzi), felixb@tlvmc.gov.il (F. Bokstein), deborahblumenthal@gmail.com (D.T. Blumenthal), Ornaaizenstein@gmail.com (O. Aizenstein), giladliberman@gmail.com (G. Liberman), bencorn@tlvmc.gov.il (B.W. Corn), dafnab@tlvmc.gov.il (D. Ben Bashat).
[1] Tel.: +972 50 6868307; fax: +972 3 6973080.
[2] Tel.: +972 52 4266532; fax: +972 3 6973080.
[3] Tel.: +972 52 4266304; fax: +972 3 6973080.
[4] Tel.: +972 52 4266611; fax: +972 3 6973080.
[5] Tel.: +972 52 3891380; fax: +972 3 6973080.
[6] Tel.: +972 52 4266533; fax: +972 3 6973080.

http://dx.doi.org/10.1016/j.ejrad.2014.03.026
0720-048X/

1. Introduction

Glioblastoma (GB) is the most aggressive brain tumor type and despite advances in frontline therapy, the majority of GB patients have a poor prognosis [1]. Bevacizumab, a monoclonal antibody to vascular endothelial growth factor (VEGF), was approved in 2009 by the FDA for the treatment of recurrent GB [2]. Early magnetic resonance imaging (MRI) based studies reported an initially rapid and remarkable radiologic response, with 25–60% reduction in the size of the contrast-enhanced tumor and hyperintense fluid attenuated inversion recovery (FLAIR) areas, detected in the majority of patients as early as 1 to 2 days after initiation of therapy [3–5]. It has been suggested that this initial response may be partly due to the normalization of the abnormally permeable tumor vessels and not always indicative of an anti-glioma effect [3]. Several studies have demonstrated that following bevacizumab therapy, GB is more likely to progress with an infiltrative tumor pattern, characterized by an increase in the non-enhancing component as detected by T_2-weighted imaging (WI) and FLAIR [3–5].

In an attempt to better assess therapy response in the context of bevacizamab use, radiological criteria have been expanded, and a new classification system, the Response Assessment in Neuro-Oncology [RANO] [3] criteria, have been developed, based on recognition of changes in the T_2WI/FLAIR signal in addition to changes in the T_1WI contrast enhanced signal. However, it is not always clear if these changes indicate tumor progression (as non enhancing infiltrative tumor) or non-tumoral *vasogenic-edema* [6,7].

Several studies have proposed methods for automatic or semi-automatic segmentation and quantification of brain tumor components in patients with GB based on multi-parametric MR data [8–10]. Only a few studies have attempted to classify the non-enhancing lesion area in order to identify infiltrative tumor area, using conventional imaging [8] or diffusion tensor imaging (DTI) [11,12]. However, using DTI, contradictory results were reported [11,12], and there was only limited use of advanced imaging methods for tissue classification and characterization, in particular, vascular imaging methods.

The aim of this study was to identify the infiltrative tumor areas within the non-enhancing FLAIR lesion area, indicating disease progression in patients with GB following bevacizumab therapy. Multiparametric MRI was employed, including conventional, diffusion and vascular imaging methods, in order to provide a more accurate assessment of therapy response. The non-enhancing FLAIR lesion area was classified into *vasogenic-edema* and *tumor-infiltrative* areas based on imaging characteristics, and longitudinal changes in these two components were assessed throughout bevacizumab therapy.

2. Methods

2.1. Subjects

Fourteen patients with biopsy-confirmed GB (8 men, 52 ± 2 years) who received bevacizumab, were scanned prospectively, longitudinally with an identical MRI protocol including conventional, diffusion and dynamic susceptibility contrast (DSC) imaging (total of 40 MR scans). All patients had been treated with standard therapies of surgery, radiation and chemotherapy prior to bevacizumab therapy. Three patients (patients number 1 and 3) had received carboplatin/etoposide as second-line therapy prior to receiving third-line bevacizumab with irinotecan. Bevacizumab was infused intravenously at doses of 5 or 10 mg/kg every 2 weeks. In some cases the bevacizumab was given concurrently with irinotecan or temozolomide and in some cases, as monotherapy. Detailed information for each patient is given in Table 1. The study was approved by the hospital review board, and written informed consent was obtained from all patients.

2.2. MRI protocol

MRI scans were performed on a 3.0T MRI scanner (GE Signa EXCITE). The protocol included anatomical sequences: T_1WI performed before and after contrast agent injection (Gadolinium-Dotarem (Gad)) (T_1WI/T_1WI + Gad), T_2WI, and FLAIR. In addition, DSC, dynamic contrast enhancement (DCE), DTI and MR-spectroscopy (MRS) were performed. DSC data was acquired using a gradient echo-EPI sequence during the injection of 0.4 cm^3/kg Gad, using a power injector (MEDRAD, Spectris Solaris EP), at a constant rate of 5 cm^3/s. Other imaging parameters included: field of view (FOV)/matrix = 220 mm/128 × 128, repetition time (TR)/echo time (TE) = 1300/30 ms. DCE data was acquired in nine patients (28 MRI scans). First, T_1 maps were calculated based on the variable flip angle spoiled SPGR (VFA-SPGR) method. Next, multi phase 3D T_1WI SPGR images were acquired before, during and after the injection of 0.2 cm^3/kg Gad, at a constant rate of 5 cm^3/s. Other scan parameters were: FOV/matrix = 250 mm/256 × 256, TR/TE = 5.68/1.24 ms, flip angles (FA) = 5°/10°/15°/25° for the VFA-SPGR volumes, and 20° for the multi-phase data. The DTI was acquired along 15 co-linear diffusion gradient directions (b = 0, 1000 s/mm^2) with FOV/matrix = 220 mm/128 × 128, TR/TE = 8000/95 ms. The MRS data was acquired using 2D multi-voxel PRESS CSI sequence, with 16 × 16 transverse phase encoding matrix, TR/TE = 1500/144 ms, placed at the center of the lesion area.

2.3. Image analysis

The non-enhancing FLAIR lesion area was classified into *vasogenic-edema* and *tumor-infiltrative* areas, as follows:

2.3.1. Data preprocessing

Preprocessing was performed using FMRIB Software Library (FSL, www.fmrib.ox.ac.uk/fsl); SPM5 and Freesurfer (www.nitrc.org/projects/freesurfer) and included; skull stripping; realignment of all images and calculated maps to the FLAIR image; one millimeter smoothing and B_1 inhomogeneity correction [13] applied to the anatomical images.

2.3.2. Map calculation

Mean diffusivity (MD) and fractional anisotropy (FA) maps were calculated using FSL diffusion tool. cerebral blood volume and flow (CBV, CBF) maps were calculated using perfusion graphical user interface software (Penguin). Maps of T_1WI enhancement (EnT_1WI) were calculated after intensity normalization (see below), as: EnT_1WI map = T_1IW + Gad/T_1IW × 100. Plasma volume (V_p) and volume transfer constant (k^{trans}) maps were calculated from the DCE data, based on Tofts model [14], using in-house code written in MATLAB.

2.3.3. Intensity normalization

Normalization of the FLAIR, T_1WI, T_1WI + Gad, CBV and CBF maps was performed relative to the mean value obtained at the reference normal appearing white matter (NAWM) area defined separately in each data set (see below).

2.3.4. Brain segmentation

Segmentation of brain tissue was performed in order (1) to identify the target area for classification (i.e. the non-enhancing hyper intense FLAIR area), and (2) to define the reference area for normalization (the NAWM) area in the contralesional hemisphere,

Table 1
Patient characteristics.

Patient	Gender	Age (years)	Enhancing tumor volume (ml)	Non-enhancing lesion—volume (ml)	Enhancing tumor—anatomical location	Chemotherapy	Chemo cycles	PFS (days)	MRI scans (weeks)
1	Male	51	30	128	LT, LO	BVZ 10 mg/kg + TMZ	6	147	0, 24
2	Female	67	21	159	RP, RO	BVZ 5 mg/kg only	13	182	0, 8, 24
3	Male	43	10	78	RP, RT	BVZ 10 mg/kg + TMZ	19	720	0, 2, 24
4	Male	42	44	131	RT, RO	BVZ 10 mg/kg + CPT	6	231	0, 2, 8, 16
5	Female	51	3	58	LF	BVZ 10 mg/kg + TMZ	17	259	0, 8, 24
6	Female	60	7	111	LO	BVZ 10 mg/kg + CPT	13	420	0, 2, 8, 16
7	Male	41	8	86	L F, LP	BVZ 10 mg/kg only	8	127	0, 8, 24
8	Male	45	28	121	L T	BVZ 10 mg/kg + CPT	12	174	0, 2, 8
9	Female	62	17	141	LT, LO	BVZ 10 mg/kg + TMZ	7	141	0, 2, 8
10	Female	74	57	93	RO	BVZ 10 mg/kg + CPT	4	47	0, 2, 8
11	Female	70	59	115	RF	BVZ 10 mg/kg + TMZ	7	84	0, 2, 8
12	Male	34	108	212	LF, LP	BVZ 5 mg/kg + CPT	37	99	0, 16
13	Female	68	62	167	LT	BVZ 10 mg/kg + TMZ	6	90	0, 2
14	Male	39	67	132	LT	BVZ 10 mg/kg + CPT	4	60	0, 2

PFS = progression-free survival; BVZ = bevacizumab; CPT = irinotecan; TMZ = temozolomide; volumes = in ml at baseline; R = right; L = left; F = frontal lobe; P = parietal lobe; T = temporal lobe; O = occipital lobe.

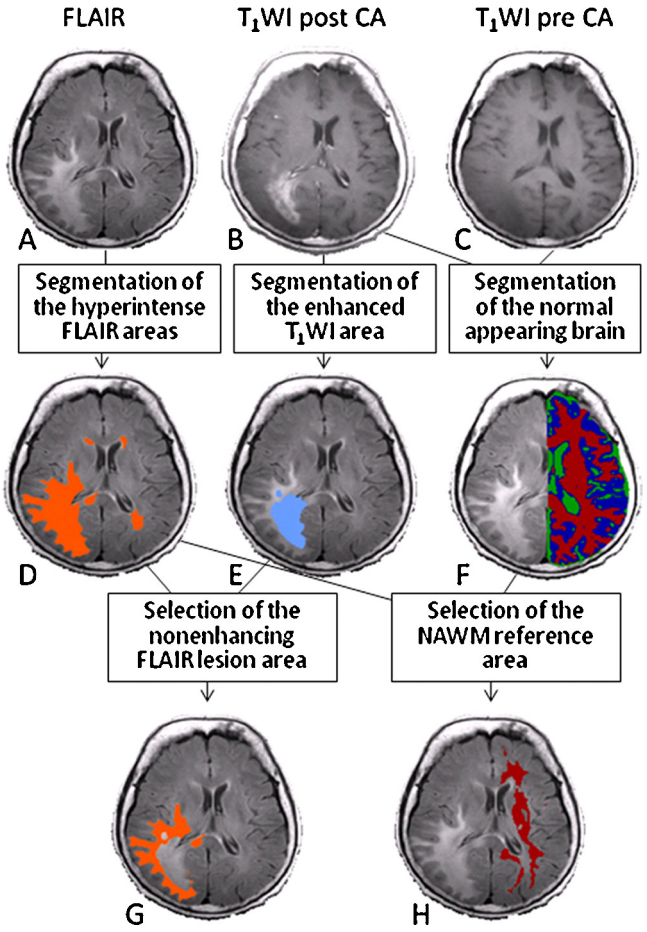

Fig. 1. Brain tissue segmentation. Anatomical images used for tissue segmentation: (A) fluid attenuation inversion recovery (FLAIR), (B) T_1WI acquired after contrast agent injection (T_1WI + GAD), (C) T_1WI acquired before contrast agent injection (T_1WI), (D) the identified hyperintense FLAIR area (orange), (E) the identified enhancement T_1WI lesion area (light blue), (F) segmentation of the hemisphere contra lateral to the tumor into gray matter (blue), white mater (red) and cerebral spinal fluid (green). (G) The obtained non-enhancing FLAIR lesion area (orange), (H) The obtained NAWM reference area (red). (For interpretation of the references to color in this figure legend, the reader is referred to the web version of this article.)

defined separately in each modality (Fig. 1). The hyper intense FLAIR area and the enhanced T_1WI area were identified via an unsupervised brain segmentation method using FSL segmentation tool (FAST) [15], based on a previously described methodology [16]. The target area for classification (the non-enhancing FLAIR lesion area) was defined by subtracting the enhanced T_1WI area from the hyper intense FLAIR area. The reference area for normalization was defined separately for each modality as the NAWM at the contralesional hemisphere, using unsupervised *k*-mean segmentation with $k = 3$ [16] and excluding areas with hyperintense FLAIR area. Normalized maps of T_1WI, FLAIR, CBV and CBF were calculated relative to the mean value at the reference area.

2.3.5. Multiparametric classification of lesion area

Unsupervised multiparametric clustering was performed on the non-enhancing FLAIR lesion area using the FSL segmentation tool. The input data included the MD map and the normalized CBV and CBF maps (rCBV, rCBF), with the number of tissue clusters set to five (arbitrary choice). This resulted in 5 clusters for each patient, each represented by a mean vector of three dimensions. In each patient, only voxels with probability >50% of belonging to one of the clusters were included, resulting in a total of 200 clusters from all patients (40 MRI scans $\times$ 5 clusters). Five clusters with MD values $\geq$ two standard deviations (SD) of the mean value of all clusters ($>1.87 \times 10^{-3}$ mm^2/s), were considered as cystic-necrotic component (based on visual inspection and [17]), and were therefore excluded, resulting in 195 clusters. In order to identify relatively homogeneous clusters between patients, a second classification was performed on all clusters based on their MRI fingerprint, using *k*-mean cluster analysis (SPSS 12.0, SPSS Inc., Chicago, IL, USA). Eight different numbers of *k* ($k = 3$–10) were used, and classification results were evaluated, using a multivariate analysis of variance between tissue classes with Bonferroni correction, for each *k*. The optimal *k* was chosen as the number that best differentiated between the different tissue classes, in our study $k = 3$.

One way ANOVA with Bonferroni correction for multiple comparisons was used to assess significance between the three components. The ANOVA was performed on all MRI parameters: rCBV, rCBF, MD, FA, rFLAIR, EnT_1WI, k^{trans} and V_p, (including parameters that were not used for the classification). Effect size (*ES*) was used to assess differences between component C1 + C2 and C3 (later defined as *tumor-infiltrative* and *vasogenic-edema*) as follows: $ES = (\mu_1 - \mu_2)/\sigma$. Where: μ_1 = mean of C1 + C2; μ_2 = mean of C3; σ = mean SD of C3 and C1 + C2; 0.1, 0.3 and 0.5 were considered small, medium and large effect sizes, respectively [18].

2.3.6. Data validation

Classification results were validated using MRS. Ratios of *N*-acetyl aspartate (NAA) to creatine (Cr) and choline (Cho) to Cr were calculated automatically from the area under each metabolite peak

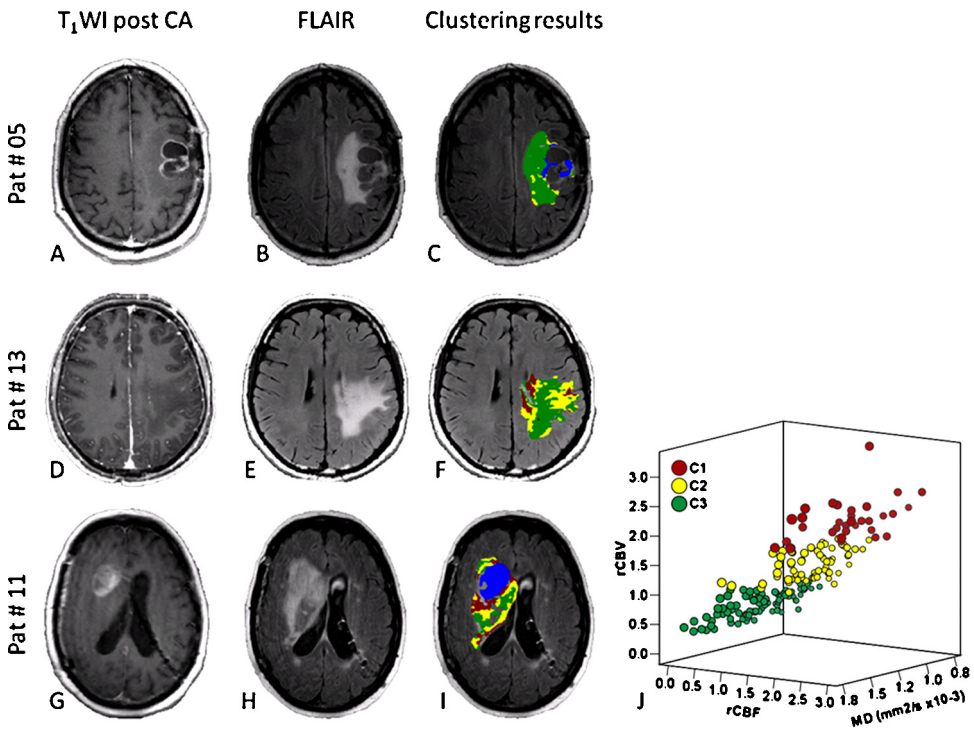

Fig. 2. Classification of the non-enhancing FLAIR lesion area obtained from three patients (Pat) scanned at baseline (before the administration of bevacizumab); T_1 WI acquired after contrast agent injection (T_1 WI + GAD) ((A), (D) and (G)); Fluid attenuation inversion recovery (FLAIR) ((B), (E) and (H)); and classification results ((C), (F) and (I)) with C1 marked in red, C2 marked in yellow and C3 marked in green. The identified enhanced T_1WI lesion area marked in blue; (J) three dimensional scatter plot of the relative cerebral blood volume and flow (rCBV, rCBF) and mean diffusivity (MD) values obtained for the three components from all subjects ($n = 14$, total of 195 clusters).

by the standard GE Functool software (GE Healthcare). Independent sample *t*-tests were used to compare the MRS results between components.

2.3.7. Correlation with progression free survival (PFS)

Correlations between PFS and the percentage of *tumor-infiltrative* volume within the total non enhancing FLAIR lesion area) were performed for each time point, using SPSS Pearson correlation.

3. Results

3.1. Classification results

The proposed methodology was successfully applied to all data sets. The volumes of the enhancing and non-enhancing FLAIR lesions and the anatomical locations of the enhancing tumor are given in Table 1. The mean volume of the enhancing tumor was 37 ± 30 ml and that of the non-enhancing lesion was 124 ± 40 ml. Three tissue types (components) were identified within the non-enhancing FLAIR lesion, statistically significantly differing by their MRI fingerprint (Table 2). Component #1 (C1) demonstrated higher rCBV, rCBF and V_p values compared with the other two components, lower rFLAIR and higher Ent$_1$WI compared with component #3 (C3). C3 demonstrated the lowest rCBV, rCBF and Ent$_1$WI values compared with the other two components/clusters; higher MD values compared with component #2 (C2) and lower V_p values compared with C1. C2 was characterized by intermediate values compared with the other two clusters, with rCBV and rCBF values higher relative to the reference areas (the NAWM in the contralesional hemisphere). A trend of increased permeability was detected between the three components with the highest k^{trans} value detected for C1, and the lowest for C3.

Fig. 2 shows representative data obtained from three patients at baseline and a scatter plot of the components obtained from all patients at all time points (total of 195 clusters) according to their rCBV, rCBF and MD values.

C3 was characterized by low rCBV and rCBF values, similar to a previously reported study characterizing vasogenic edema in patients with meningiomas [19]; therefore this component was referred to in the current study as *vasogenic-edema*. C1 and C2 showed increased rCBV, rCBF and Ent$_1$WI values relative to NAWM, and lower rFLAIR relative to C3. This pattern supported a tumoral process [20] and although these two components might indicate different degrees of proliferation/cellularity, they were combined and referred to as *tumor-infiltrative* area.

The effect size between the identified *vasogenic-edema* and *tumor-infiltrative* areas was large for rCBV, rCBF, rFLAIR and Ent$_1$WI, medium for MD and V_p and small for FA and k^{trans} (Table 2).

3.2. Validation of the classification results

Metabolite ratios were calculated from non-enhancing FLAIR lesion areas identified as either *vasogenic-edema* or *tumor-infiltrative* areas. A total of 32 spectra were obtained from fifteen scans of nine patients. The MRS findings supported the classification results, demonstrating significantly higher Cho/Cr ratio ($p < 0.001$) for the *tumor-infiltrative* ($n = 17$, 1.63 ± 0.27) compared with the *vasogenic-edema* ($n = 15$, 1.25 ± 0.27) areas.

3.3. Follow up of patients during bevacizumab therapy

In most patients, as expected, reductions were detected both in the T_1WI enhanced tumor area (T_1WI + Gad) and in the hyperintense FLAIR lesion areas during the course of therapy. The most significant changes were observed during the first weeks following therapy initiation, with a mean reduction of $58 \pm 10\%$ for the enhanced T_1WI + Gad areas and $53 \pm 9\%$ for the hyperintense FLAIR

Table 2
MRI parameters obtained for the different components.

Components	rCBV* (a.u)	rCBF* (a.u)	MD* ($mm^2/s \times 10^{-3}$)	FA* (a.u)	rFLAIR* (a.u)	EnT_1WI* (%)	k^{trans}** ($1/min \times 10^{-3}$)	V_p** (a.u)
C1	2.28 ± 0.34^a	2.23 ± 0.32^a	1.28 ± 0.27	0.23 ± 0.05	1.32 ± 0.10^b	5.79 ± 3.53^b	1.24 ± 1.64	3.81 ± 4.23^a
C2	1.38 ± 0.25^a	1.34 ± 0.23^a	1.16 ± 0.23^b	0.26 ± 0.06	1.33 ± 0.09^b	4.94 ± 3.88^b	0.65 ± 1.23	1.85 ± 2.26^c
C3 [*Vasogenic-edema*]	0.71 ± 0.20^a	0.66 ± 0.20^a	1.29 ± 0.26^d	0.24 ± 0.06	1.41 ± 0.13^a	3.43 ± 3.14^a	0.59 ± 1.09	1.58 ± 1.76^c
C1 + C2 [*Tumor-infiltrative*]	1.68 ± 0.51	1.64 ± 0.50	1.20 ± 0.25	0.25 ± 0.06	1.32 ± 0.09	5.22 ± 3.77	0.84 ± 1.39	2.48 ± 3.14
ES	**2.73**	**2.80**	−0.35	0.17	**−0.82**	**0.52**	0.20	0.37

rCBV/rCBF = relative cerebral blood volume and flow; MD = mean diffusivity; FA = fractional anisotropy; a.u. = arbitrary units; rFLAIR = relative fluid attenuation inversion recovery. Number of clusters in each component:

* C1: $n = 34$; C2: $n = 68$; C3: $n = 93$

** C1: $n = 23$; C2: $n = 43$; C3: $n = 66$. Significant differences were assessed only between C1, C2 and C3; significant differences ($p < 0.01$, corrected). *ES* = effect size between the *vasogenic-edema* (C3) and *tumor-infiltrative area* (C1 + C2); large *ES* are marked in bold.

[a] Compared with the other two components.
[b] Compared with C3 component.
[c] Compared with C1 component.
[d] Compared with C2 component.

lesion areas, detected between baseline and the first MRI following therapy initiation.

Longitudinal changes of the *vasogenic-edema* and *tumor-infiltrative* areas were assessed in 10 patients (who had more than two MRI scans) relative to their first MRI after treatment initiation. The *vasogenic-edema* volume demonstrated longitudinal reduction during therapy in 7/10 patients, while in the other three patients the volume only slightly increased (less than 10%) or did not change. The *tumor-infiltrative* area increased in 7/10 patients, while in two patients there was no change, and only in one patient a reduction in the volume of this component was detected.

Out of the seven patients who demonstrated an increase in the *tumor-infiltrative* area, five showed also increases both in the enhancing tumor volume and in the total FLAIR lesion area (obvious tumor progression); one patient showed a reduction in the enhancing tumor volume yet an increase in the volume of the total FLAIR lesion area (tumor progression based on RANO criteria) and one patient showed a reduction in both the enhancing tumor volume and the FLAIR lesion area (likely disease progression with a shift to an infiltrative pattern of tumor progression).

Representative longitudinal data obtained from three patients (number 6, 8, and 10), is shown in Fig. 3. In two patients (number 8 and 10), changes in hyperintense FLAIR lesion area can be seen throughout therapy, manifested by a substantial reduction of the *vasogenic-edema* (green), and an increase in the *tumor-infiltrative* areas (orange); essentially, a clear directional shift to an infiltrative pattern of tumor progression. One patient (number 6) showed stable disease, with almost no change in the hyperintense FLAIR lesion volume, and no changes in the volume of the two components.

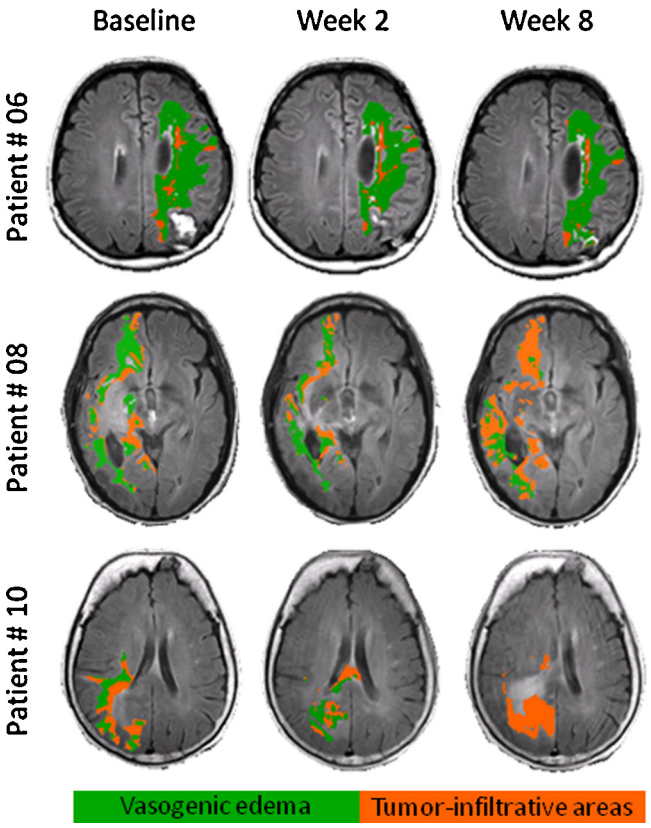

Fig. 3. Classification results of the non-enhancing FLAIR lesion area during therapy obtained from three patients at baseline, two and eight weeks following initiation of bevacizumab therapy.

3.4. Correlation with PFS

The PFS of each patient is given in Table 1 (patient characteristics). No significant correlations were detected between PFS and the percentage of *tumor-infiltrative* volume detected at baseline ($n = 14$) and at week 2 ($n = 9$). Significant correlations were detected between PFS and the percentage of *tumor-infiltrative* volume detected at week 8 ($n = 9$, $r = -0.86$, $p = 0.003$) and week 16 ($n = 5$, $r = -0.99$, $p = 0.001$), indicating that an increase in the *tumor-infiltrative* volume correlates with reduction of the PFS.

4. Discussion

This study characterizes the non-enhancing hyperintense FLAIR lesion area in patients with GB, indicating a shift to an infiltrative pattern of tumor progression following bevacizumab therapy in most patients, and provides MR-based biomarkers for prediction of PFS. Longitudinal follow up demonstrates tumor progression in most patients, as detected by a decrease in *vasogenic-edema*, accompanied by an increase in *tumor-infiltrative* area. These changes, detected in patients who demonstrate an increase in enhancing tumor volume and/or in the hyperintense FLAIR lesion area, clearly support the use of RANO criteria. In addition, increase in the *tumor-infiltrative* area can occur when there is no increase in the enhancing tumor volume or in the overall hyperintense FLAIR lesion area. The proposed method may improve therapy response assessment in patients with GB treated with anti-angiogenic therapies.

The non-enhancing FLAIR lesion components were identified using unsupervised multiparametric classification, resulting in three distinct tissue types which could be differentiated by their MR fingerprint. The classification into three components was based on statistical optimization. C3 was referred to in this study as *vasogenic-edema*, mainly based on its vascular characteristics. This

pattern of reduced CBV and CBF has been previously demonstrated in several studies of brain tumors in both patients [20,21] and animal models [22], and can be explained by the compression of the capillaries by vasogenic edema [19]. In addition, this component had higher rFLAIR values compared with the other two components, indicating an increase in T_2 relaxation time, which was shown to correlate with tissue water fraction [7]. Both C1 and C2 demonstrated infiltrative tumor patterns, most likely representing different degrees of proliferation or cellularity. In order to simplify these MR-based biomarkers as tools for the assessment of therapy response, C1 and C2 were combined and referred to as *tumor-infiltrative*. This definition was supported by previous studies that reported an association between the peritumoral hyperintensity T_2WI/FLAIR areas in high grade gliomas, the tumor infiltration boundaries, and increased rCBV values compared with the NAWM [20,23].

The classification results were validated using MRS, with significantly higher Cho/Cr values detected in the *tumor-infiltrative* area. Brain metabolite concentrations were shown to be correlated with histopathological analyses in previous research [24] and to be sensitive for the detection of tumor progression, supporting the use of MRS for diagnosis and evaluation of treatment response in human brain tumors [4,24].

Previous studies suggested that GB rapidly adapts to anti-angiogenic therapy, eventually leading to infiltrative tumor progression with clinical progression [5]. It was suggested that anti-VEGF therapy may increase the tendency of tumor cells for co-option to existing blood vessels, resulting in an invasive, non-enhancing phenotype [25].

A pattern of rapid tumor recurrence and revascularization has been noted both in animal models using fluorescence imaging [26], and in patients, based on conventional MRI [27]. Results from this study show that following bevacizumab therapy, an increase either in the enhanced tumor volume and/or in the hyperintense FLAIR lesion area was associated with increase in the *tumor-infiltrative* area, indicating tumor progression, thus supporting the use of RANO criteria. In addition, preliminary results in one patient showed an increase in the *tumor-infiltrative* area, without increase in the enhancing tumor and/or the FLAIR lesion volumes. This may indicate disease progression not identified by traditional imaging methods, and may be important for therapy response assessment.

Correlations to PFS were not significant at baseline or at week 2, indicating that neither baseline disease severity nor initial radiological response indicate long term therapy response. However significant correlations were detected between PFS and the percentage of *tumor-infiltrative* volume detected at week 8 and week 16. These results indicate that identification and quantification of the *tumor-infiltrative* volume at these time points may provide MR biomarkers for therapy response assessment. Yet, further studies with a larger sample size are needed to confirm these findings.

The imaging parameters that contribute most to differentiation between the tissue components were CBV and CBF, two vascular parameters extracted from DSC. In addition, the *tumor-infiltrative* area was characterized by higher k^{trans} and V_p [14] compared with the *vasogenic-edema*. These findings emphasize the importance of using vascular imaging in the assessment and follow up of bevacizumab therapy response.

DTI parameters (both MD and FA) were not significantly different between the *vasogenic-edema* and *tumor-infiltrative* areas. Previous studies showed inconsistent results regarding the capability of diffusion imaging in differentiating *vasogenic-edema* from *tumor-infiltrative* area [11,12,28]. These results, together with our findings, suggest that diffusion imaging alone may not be sensitive enough to differentiate between *vasogenic-edema* and *tumor-infiltrative* area in patients following bevacizumab therapy.

While this study relates the imaging characteristics to the effect of bevacizumab, previous therapies (post surgical, post radiation, etc) could also have long term effects. Long term radiation effects were shown to induce BBB disruption (as detected by DCE), fractional anisotropy reduction (as detected by DTI) and decrease of NAA/Cr and Cho/Cr ratios (as detected by MRS) [29]. Thus, it may be difficult to differentiate between *vasogenic-edema* and delayed radiation WM changes that may have similar radiological appearances. Yet, the *infiltrative-tumor* component was characterized mainly by increased rCBV and rCBF, which are not expected following radiation, along with high Cho/Cr ratio, which was previously shown to correlate with the degree of tumor infiltration [24]. Therefore, this pattern is not likely to be associated with late therapy effects, but rather represents a tumor infiltrative progression pattern occurring under bevacizumab therapy.

Several limitations to this study should be considered. The associations between the obtained components and tissue type (i.e. *vasogenic-edema*/*tumor-infiltrative* area) were based on MRI characteristics that were supported by MRS in 9/15 patients. Although several cases showed good correlation between 1H-MRS and the degree of tumor infiltration, as detected by quantitative histopathological analysis in previous studies [24,30], future studies (including animal models and/or post mortem studies) are needed to provide direct histological validation of our findings. In addition, this study had a relatively small sample size, however, despite the small number of patients included in this study, there was a relatively large number of MRI scans, and highly significant differences were detected between the tissue clusters (195 clusters), strengthening the statistical power of the study. Some variability in MRI parameters was evident, as generally seen with bevacizumab, and manifested by the relatively high SD values, yet the effect sizes between the *vasogenic-edema* and *tumor-infiltrative* area were large in all parameters used for classification.

5. Conclusion

Increase in the hyperintense FLAIR lesion volume following bevacizumab therapy was associated with increase in the *infiltrative-tumor* area, suggested to indicate tumor progression. In addition, a shift to *infiltrative-tumor* pattern can be detected in patients who show no increase in the hyperintense FLAIR lesion volume. The identification of the *infiltrative-tumor* area can be achieved primarily by vascular imaging, which is recommended to be included as standard follow-up assessment in this patient population. Identification of changes in the *infiltrative-tumor* area within the non-enhancing hyperintense FLAIR lesion area in patients with GB, may improve therapy response assessment following bevacizumab therapy.

Conflict of interest statement

We wish to confirm that there are no potential financial interests associated with the publication of this paper on the part of any of the authors and there has been no significant financial support for this work that could have influenced its outcome.

Funding

This work was supported by the James S. McDonnell Foundation number 220020176.

Acknowledgments

To Vicki Myers for editorial assistance and to Guy Nadav for technical support. This work was performed in partial fulfillment of

the requirements for a Ph.D. degree of Artzi Moran, Sackler Faculty of Medicine, Tel Aviv University, Israel.

References

[1] Wen PY, Kesari S. Malignant gliomas in adults. N Engl J Med 2008;359(5):492–507.
[2] Weller M, Cloughesy T, Perry JR, Wick W. Standards of care for treatment of recurrent glioblastoma—are we there yet? Neuro Oncol 2013;15(1):4–27.
[3] Wen PY, Macdonald DR, Reardon DA, et al. Updated response assessment criteria for high-grade gliomas: response assessment in neuro-oncology working group. J Clin Oncol 2010;28(11):1963–72.
[4] Pope WB, Young JR, Ellingson BM. Advances in MRI assessment of gliomas and response to anti-VEGF therapy. Curr Neurol Neurosci Rep 2011;11(3):336–44.
[5] de Groot JF, Fuller G, Kumar AJ, et al. Tumor invasion after treatment of glioblastoma with bevacizumab: radiographic and pathologic correlation in humans and mice. Neuro Oncol 2010;12(3):233–42.
[6] Hattingen E, Jurcoane A, Daneshvar K, et al. Quantitative T2 mapping of recurrent glioblastoma under bevacizumab improves monitoring for non-enhancing tumor progression and predicts overall survival. Neuro Oncol 2013;15(10):1395–404.
[7] Ellingson BM, Cloughesy TF, Lai A, et al. Quantification of edema reduction using differential quantitative T2 (DQT2) relaxometry mapping in recurrent glioblastoma treated with bevacizumab. J Neurooncol 2012;106(1):111–9.
[8] Liberman G, Louzoun Y, Aizenstein O, et al. Automatic multi-modal MR tissue classification for the assessment of response to bevacizumab in patients with glioblastoma. Eur J Radiol 2013;82(2):e87–94.
[9] Egger J, Bauer MHA, Kuhnt D, et al. A flexible semi-automatic approach for glioblastoma multiforme segmentation. In: Proceedings of International Biosignal Processing Conference. 2010.
[10] Corso JJ, Sharon E, Dube S, El-Saden S, Sinha U, Yuille A. Efficient multilevel brain tumor segmentation with integrated bayesian model classification. IEEE Trans Med Imaging 2008;27(5):629–40.
[11] Lu S, Ahn D, Johnson G, Law M, Zagzag D, Grossman RI. Diffusion-tensor MR imaging of intracranial neoplasia and associated peritumoral edema: introduction of the tumor infiltration index. Radiology 2004;232(1):221–8.
[12] Kinoshita M, Goto T, Okita Y, et al. Diffusion tensor-based tumor infiltration index cannot discriminate vasogenic edema from tumor-infiltrated edema. J Neurooncol 2010;96(3):409–15.
[13] Sled JG, Zijdenbos AP, Evans AC. A nonparametric method for automatic correction of intensity nonuniformity in MRI data. IEEE Trans Med Imaging 1998;17(1):87–97.
[14] Tofts PS, Kermode AG. Measurement of the blood-brain barrier permeability and leakage space using dynamic MR imaging. 1. Fundamental concepts. Magn Reson Med 1991;17(2):357–67.
[15] Zhang Y, Brady M, Smith S. Segmentation of brain MR images through a hidden Markov random field model and the expectation-maximization algorithm. IEEE Trans Med Imaging 2001;20(1):45–57.
[16] Artzi M, Aizenstein O, Jonas-Kimchi T, Myers V, Hallevi H, Ben Bashat D. FLAIR lesion segmentation: application in patients with brain tumors and acute ischemic stroke. Eur J Radiol 2013;82(9):1512–8.
[17] Hakyemez B, Erdogan C, Yildirim N, Parlak M. Glioblastoma multiforme with atypical diffusion-weighted MR findings. Br J Radiol 2005;78(935):989–92.
[18] Cohen J. A power primer. Psychol Bull 1992;112(1):155–9.
[19] Kaal EC, Vecht CJ. The management of brain edema in brain tumors. Curr Opin Oncol 2004;16(6):593–600.
[20] Law M, Cha S, Knopp EA, Johnson G, Arnett J, Litt AW. High-grade gliomas and solitary metastases: differentiation by using perfusion and proton spectroscopic MR imaging. Radiology 2002;222(3):715–21.
[21] Uematsu H, Maeda M, Itoh H. Peritumoral brain edema in intracranial meningiomas evaluated by dynamic perfusion-weighted MR imaging: a preliminary study. Eur Radiol 2003;13(4):758–62.
[22] Hossman KA, Bloink M. Blood flow and regulation of blood flow in experimental peritumoral edema. Stroke 1981;12(2):211–7.
[23] Senturk S, Oguz KK, Cila A. Dynamic contrast-enhanced susceptibility-weighted perfusion imaging of intracranial tumors: a study using a 3T MR scanner. Diagn Interv Radiol 2009;15(1):3–12.
[24] Croteau D, Scarpace L, Hearshen D, et al. Correlation between magnetic resonance spectroscopy imaging and image-guided biopsies: semiquantitative and qualitative histopathological analyses of patients with untreated glioma. Neurosurgery 2001;49(4):823–9.
[25] Abramovitch R, Dafni H, Smouha E, Benjamin LE, Neeman M. In vivo prediction of vascular susceptibility to vascular susceptibility endothelial growth factor withdrawal: magnetic resonance imaging of C6 rat glioma in nude mice. Cancer Res 1999;59(19):5012–6.
[26] Mancuso MR, Davis R, Norberg SM, et al. Rapid vascular regrowth in tumors after reversal of VEGF inhibition. J Clin Invest 2006;116(10):2610–21.
[27] Zuniga RM, Torcuator R, Jain R, et al. Rebound tumour progression after the cessation of bevacizumab therapy in patients with recurrent high-grade glioma. J Neurooncol 2010;99(2):237–42.
[28] Gerstner ER, Frosch MP, Batchelor TT. Diffusion magnetic resonance imaging detects pathologically confirmed, nonenhancing tumor progression in a patient with recurrent glioblastoma receiving bevacizumab. J Clin Oncol 2010;28(6):e91–3.
[29] Greene-Schloesser D, Robbins ME, Peiffer AM, Shaw EG, Wheeler KT, Chan MD. Radiation-induced brain injury: a review. Front Oncol 2012;2:73.
[30] Gupta RK, Cloughesy TF, Sinha U, et al. Relationships between choline magnetic resonance spectroscopy, apparent diffusion coefficient and quantitative histopathology in human glioma. J Neurooncol 2000;50(3):215–26.